Neuron

Article

Amyloid induced hyperexcitability in default mode network drives medial temporal hyperactivity and early tau accumulation

Highlights

- Local Alzheimer's pathology disrupts excitatory-inhibitory balance
- Directed hyperexcitation links spatially disparate Alzheimer's pathologies
- This directed hyperexcitation predicts early tau accumulation

Authors

Joseph Giorgio, Jenna N. Adams, Anne Maass, William J. Jagust, Michael Breakspear

Correspondence

jgiorgio@berkeley.edu

In brief

The core pathologies of Alzheimer's disease (AD) arise in spatially distinct areas of the brain. We provide a mechanistic account for how this occurs, showing that local AD pathology impacts the function of brain networks. This dysfunction in cortical processing cascades across the brain, precipitating further pathological changes.

Giorgio et al., 2024, Neuron *112*, 676–686
February 21, 2024
https://doi.org/10.1016/j.neuron.2023.11.014

CellPress

CellPress
OPEN ACCESS

Neuron

Article

Amyloid induced hyperexcitability in default mode network drives medial temporal hyperactivity and early tau accumulation

Joseph Giorgio,[1,2,6,*] Jenna N. Adams,[3] Anne Maass,[4] William J. Jagust,[1] and Michael Breakspear[2,5]
[1]Helen Wills Neuroscience Institute, University of California, Berkeley, Berkeley, CA 94720, USA
[2]School of Psychological Sciences, College of Engineering, Science, and the Environment, University of Newcastle, Newcastle, NSW 2305, Australia
[3]Department of Neurobiology and Behavior, University of California, Irvine, Irvine, CA 92697, USA
[4]German Center for Neurodegenerative Diseases (DZNE), Magdeburg 39120, Germany
[5]Discipline of Psychiatry, College of Health, Medicine, and Wellbeing, The University of Newcastle, Newcastle, NSW 2305, Australia
[6]Lead contact
*Correspondence: jgiorgio@berkeley.edu
https://doi.org/10.1016/j.neuron.2023.11.014

SUMMARY

In early Alzheimer's disease (AD) β-amyloid (Aβ) deposits throughout association cortex and tau appears in the entorhinal cortex (EC). Why these initially appear in disparate locations is not understood. Using task-based fMRI and multimodal PET imaging, we assess the impact of local AD pathology on network-to-network interactions. We show that AD pathologies flip interactions between the default mode network (DMN) and the medial temporal lobe (MTL) from inhibitory to excitatory. The DMN is hyperexcited with increasing levels of Aβ, which drives hyperexcitability within the MTL and this directed hyperexcitation of the MTL by the DMN predicts the rate of tau accumulation within the EC. Our results support a model whereby Aβ induces disruptions to local excitatory-inhibitory balance in the DMN, driving hyperexcitability in the MTL, leading to tau accumulation. We propose that Aβ-induced disruptions to excitatory-inhibitory balance is a candidate causal route between Aβ and remote EC-tau accumulation.

INTRODUCTION

Alzheimer's disease (AD) is characterized by the spatially distinct evolution of two pathological proteins, β-amyloid (Aβ), and aggregates of tau (as neurofibrillary tangles).[1] The primary event in AD is thought to be the aggregation of Aβ plaques within medial parietal and frontal neocortex, key hubs of the default mode network (DMN).[2,3] It has been proposed that this Aβ then promotes the migration of tau[4,5] from the transentorhinal regions of the medial temporal lobe (MTL), where it deposits in most older individuals, into lateral temporal and other neocortical regions,[6] leading to the expression of AD. How these pathologies interact across spatially distinct regions[7] is not well understood.

One putative mechanism driving these events is a causal link between Aβ and neuronal hyperexcitability. Impaired inhibitory GABAergic interneuron function, abnormal glutamate release and reuptake, and dysfunction of ion channels are all associated with localized Aβ.[8–10] This impairment in normal excitatory control and interneuron inhibition disrupts local excitatory-inhibitory (E-I) balance, triggering hyperexcitability. This local E-I imbalance likely occurs well before the clinical manifestations of AD because Aβ accumulation precedes clinical impairment by decades and drives tau spread that is most closely associated with cognitive impairment.[11,12] Given the association between prolonged neuronal stimulation and tau hyperphosphorylation,[13–15] cortical hyperexcitability due to E-I imbalance may be the missing link between Aβ and early tau deposition.

Functional MRI (fMRI) studies have shown hyperactivation in the medial parietal lobe in the early clinical stages of AD.[16,17] Similarly, hyperactivity within the MTL may follow the deposition of Aβ[18] and is observed in cognitively normal adults with evidence of primary deposition of tau in the MTL.[19–24] These human studies converge with the murine literature showing pathology-related hyperactivity.[8–10]

The presence of neuronal hyperactivity associated with AD neuropathology lends itself to empirical testing using paradigms sensitive to an E-I imbalance. For example, a candidate approach is to employ a task typically associated with suppression of neuronal activity. Here, participants viewed brief streams of visual stimuli and had to respond as to whether each stimulus was repeated or novel. This task requires learning the statistical regularities in the (visual) environment and recognizing when stimuli meet expectations. This task is reliant on repetition suppression, a classical experimental manipulation whereby cortical activity is typically reduced when subjects view a stimulus the second time.[25–27] This short-term suppression of neuronal

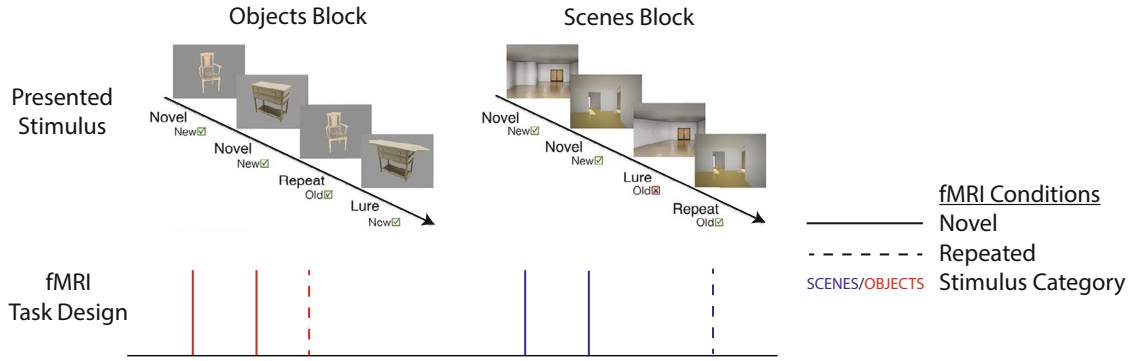

Figure 1. Task design

Top panel shows example object (left) and scene (right) blocks presented during acquisition of fMRI data. Blocks consisted of two novel stimuli, then either a highly similar lure or a repeat of one of the first two stimuli. The green tick next to each trial represents the correct discrimination for novel vs. repeated stimuli, the red cross shows an incorrect response to a lure stimulus. Bottom panel shows the fMRI task design with the modeled stimuli for each condition. fMRI design included stimuli category, either objects (red lines) or scenes (blue lines), and repetition (dashed lines).

activity represents an efficient coding strategy that minimizes metabolic cost (i.e., inhibition) to redundant information based on the statistical regularity of the environment.[28,29] Previous studies have documented deficits in repetition suppression for patients with AD and cognitively normal older adults (OAs) with AD pathology,[30–33] providing a framework to examine how E-I imbalance could affect Aβ-tau interactions. Here, using task-based fMRI and multimodal PET imaging, we assess the impact of AD pathology on network-to-network interactions, focusing on the spatial distributions of Aβ and tau accumulation. We use dynamic causal modeling (DCM) to assess the network level interactions underlying repetition suppression. We hypothesize that in the absence of Aβ pathology, repetition suppression will be associated with afferent inhibition of the DMN. However, for individuals with Aβ pathology, this inhibition will be shifted toward excitation such that Aβ-related excitation in DMN will, in turn, excite medial temporal regions driving tau accumulation.

RESULTS

Participants, task, and fMRI design

Seventy-two participants (50 cognitively normal OAs, 22 young adults [YAs]) underwent task fMRI. In the scanner, participants viewed blocks of four stimuli of either objects or scenes with the first two stimuli within a block novel and the next two stimuli either the same or a similar "lure" stimulus.[30,34,35] Participants responded on each trial indicating if the stimulus was either old (i.e., a repetition) or new (i.e., a novel or lure stimulus). A sample of 45 cognitively normal OA and 21 YA were included in the subsequent analysis of task-based fMRI data, these participants passed fMRI quality control and were able to successfully perform the mnemonic discrimination task (see STAR Methods for further details on exclusion). We modeled stimulus blood-oxygen-level-dependent (BOLD) responses using a general linear model (GLM), including novel and repeated stimuli omitting lure trials for each stimulus category (Figure 1).

In addition, 42 of the OA underwent [^{18}F]Flortaucipir (FTP) and [^{11}C]Pittsburgh compound B (PiB) PET to measure entorhinal cortex (EC) tau and neocortical Aβ. 32 of these OA participants also had measurements of longitudinal FTP-PET to examine rates of EC-tau accumulation (Table 1). The sample with molecular imaging was well balanced in regard to Aβ positivity (50% Aβ positive) and both groups of participants had some degree of EC-tau burden (FTP-standardized uptake value ratio [SUVR]: Aβ− mean ± SD = 1.26 ± 0.19; Aβ+ mean ± SD = 1.34 ± 0.26), suggesting that the whole sample includes participants with early AD neuropathological change and participants who have some degree of tau associated with normal aging, possibly primary age-related tauopathy. The average uptake of PiB and FTP shows some overlap between the two pathologies across the cortex (Figure 2). However, although there is evidence of substantial tau burden within the EC, there is little Aβ (Figure 2, bottom row). This suggests the interactions between Aβ and EC-tau that we are investigating are remote and not due to colocalized Aβ and tau pathology in the MTL.

Functional network task activation—Spatial ICA

To extract activity from cortical networks we performed group spatial independent components analysis (ICA) on the fMRI data from the 66 participants (21 YA and 45 OA). Based on the minimum descriptive length,[36] we assigned the dimensionality of the group fMRI data as 67 components. From these, we selected five cortical networks for subsequent analysis (Figure S1) based on the following premises. We hypothesized that two low-level (stimulus-related) networks would show category-related activations (i.e., scenes or objects): an "object network" centered over the lateral occipital cortex (LOC) and a "scenes network" centered over the parahippocampal place area (PPA). To probe higher order processes, we included three additional networks: the DMN, the MTL network, and the salience network (SAL). Fitting the task GLM design to the subject level component time courses and contrasting the activity for scenes versus objects confirmed the presence of strong category-specific activity for objects > scenes for the LOC ($t(65) = -21.64$, $p < 0.001$) and scenes > objects for the PPA ($t(65) = 22.4$, $p < 0.001$) (Figure 3A). When collapsing across stimulus categories, we observed significant repetition suppression effects in the MTL ($t(65) = 10.98$, $p < 0.001$) and the DMN

Table 1. Sample descriptive statistics

Analysis	ICA		DCM	Longitudinal FTP
Age category	YA	OA	OA	OA
Sample size	21	45	42	32
Age, years (mean ± SD)	26.8 (4.50)	78.0 (6.25)	78.2 (6.38)	78.9 (4.96)
Sex, female	12	17	17	12
Education, years (mean ± SD)	16.9 (1.50)	17.0 (1.36)	17.1 (1.40)	17.0 (1.30)
APOE 4 (1 or more allele)	–	–	15[a]	13[b]
PiB DVR (mean ± SD)	–	–	1.18 (0.25)	1.18 (0.26)
Aβ+	–	–	21	16
EC-FTP SUVR (mean ± SD)	–	–	1.30 (0.23)	1.31 (0.24)
EC-FTP SUVR/year (mean ± SD)	–	–	–	0.024 (0.01)
Follow up visits (2/3/4)	–	–	–	15/15/2
			1 missing[a]	1 missing[b]

ICA column shows demographics for YA and OA used to extract task-related cortical networks from the fMRI data. DCM column shows demographics and descriptive statistics for the Aβ and tau PET markers for OA included in the DCM analysis. Longitudinal FTP column shows demographics and descriptive statistics for the OA with longitudinal FTP EC-tau. Aβ positivity is determined using a DVR threshold > 1.065.
[a]APOE 4 not available for one individual from the DCM OA sample.
[b]APOE 4 not available for one individual from the Longitudinal FTP OA sample.

(t(65) = 14.04, $p < 0.001$), and a strong repetition enhancement effect in the SAL (t(65) = −13.14, $p < 0.001$) (Figure 3B).

Interrogation of the repetition effects for the OA and YA groups independently showed repetition suppression for both groups in the MTL and DMN and repetition enhancement in the SAL (Figure S2). Contrasting repetition suppression for the OA and YA groups showed significant differences in repetition effects in the MTL (t(64) = −6.87, $p < 0.001$) and DMN (t(64) = −4.76, $p < 0.001$) but not in the SAL (t(64) = 1.82, $p = 0.073$). Further, investigating the back reconstructed component maps for the MTL and DMN for OA and YA groups independently showed highly similar spatial distribution of the underlying hemodynamic sources (Figure S3). Together, this suggests that there were no systematic differences in component estimation using spatial ICA between OA and YA and time series were robustly estimated for the underlying functional networks.

System-level processing of repetition—DCM

We next used DCM to assess cortical processing of repeated stimuli for the 42 OA who had both Aβ and EC-tau PET imaging. We used deterministic, bilinear DCM to infer directed influences among cortical regions (i.e., effective connectivity) and the modulation of this connectivity by experimental task conditions (Figure 1). Crucially, these connections can either be enhancing (excitatory) or suppressing (inhibitory), reflecting the balance of local and distant E-I balance. Informed by our GLM results, we selected the LOC and PPA as category-specific input nodes receiving input from object and scene stimuli respectively, and included the MTL, DMN, and SAL as higher order networks. For each participant we built a fully connected DCM, only excluding mutual connections between PPA and LOC. We incorporated the distributed nature of repetition suppression in the cortex by permitting repetition to modulate any connection (Figure 4A). We did not include connections between PPA and LOC because we were not interested in category-specific differences in effective connectivity when stimuli are repeated. We observed a reasonable agreement between the DCM generated BOLD time series and the observed network time series (mean ± SD $R^2 = 22.2 \pm 12.5\%$) supporting interrogation of effective connectivity parameters.

Effects of AD pathology on cortical processing of repetition—PEB

We next used parametric empirical Bayes (PEB) analyses to infer how AD pathology impacts the processing of repeated stimuli among these cortical networks. This approach entails an iterative search over reduced (“lesioned”) models to investigate the impact a DCM parameter (e.g., modulation of connectivity by stimulus repetition) has on the model fit. Using this analysis, we determined the influence of each parameter (i.e., its posterior probability [Pp]) on the overall likelihood of the model independent of pathology (i.e., common effect), as well as the effect an increase in Aβ or EC-tau has on model parameters. Informed by the spatial extent of Aβ and EC-tau, we restricted the PEB analysis to the modulation of the directed connections between the DMN and MTL (for completeness we present the full results for the PEB analysis in Figure S4).

We first observed very strong evidence of bidirectional inhibition from MTL to DMN (−0.38, $p > 0.99$) and DMN to MTL (−0.29, $p > 0.99$) when stimuli are repeated (Figure 4B). However, we observe a transition from inhibition of the DMN by the MTL to excitation (2.02, $p > 0.99$) with increasing levels of Aβ. Similarly, we observe a transition from inhibition of the MTL by the DMN to excitation (1.69, $p > 0.99$) with increasing levels of EC-tau (Figure 4C). Due to the correlation between Aβ and EC-tau ($r(40) = 0.51$, $p < 0.001$) we also reversed the order they were hierarchically entered into the PEB, observing nearly identical results. This suggests that despite their collinearity, Aβ and EC-tau have differential and specific effects, with Aβ increasing the gain of the DMN, which, in turn, overstimulates the MTL. Finally, we interrogated the effective connectivity for YA and Aβ negative OA and observed the DMN received inhibitory inputs from across the

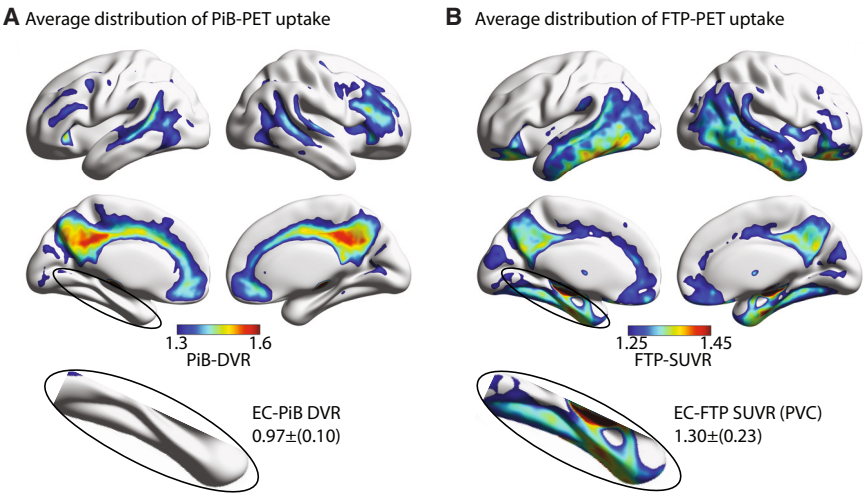

Figure 2. Spatial distribution of Aβ and tau

(A) Average distribution of PiB-PET across the cortex in Montreal Neurological Institute (MNI) space. Bottom row shows an expansion of the MTL revealing low uptake of PiB PET tracer in the EC (mean distribution volume ratio [DVR]) = 0.97 ± 0.1).

(B) Average distribution of FTP-PET across the cortex in MNI space without partial volume correction, bottom row shows an expansion of the MTL revealing high uptake of FTP-PET tracer in the EC (mean partial volume corrected SUVR = 1.30 ± 0.23).

cortex with no evidence of a transition to hyperexcitability in the DMN for the Aβ negative OA (Figure S4). This suggests that the AD-related effects between the MTL and DMN, showing a transition from inhibition to excitation, are not a feature of aging in general but rather a consequence of the transition from aging to AD pathological change.

Estimating AD pathology through directed hyperexcitation—Cross-validation analyses

We performed a series of leave one out (LOO) validation analyses to assess the generalizability of the associations between effective connectivity and Aβ and EC-tau. In these analyses we used a single PEB parameter (i.e., modulation of DMN to MTL connectivity when stimuli are repeated) to generate an out-of-sample estimation of EC-tau burden. To determine if Aβ status was a factor in this relationship, we split the 42 OA into different groups based on Aβ status (n Aβ+ = 21, n Aβ− = 21) and performed LOO cross-validation to estimate individualized EC-tau burden for each group independently. We observed that current EC-tau burden was associated with the excitation of the MTL by the DMN only in the Aβ positive sample (Aβ+ $r(19) = 0.48$, $p = 0.014$; Aβ− $r(19) = 0.20$, $p = 0.2$) (Figures 5A and 5B). Contrasting the absolute error between the estimated EC-tau burden and the observed EC-tau burden, showed a significantly better fit for the Aβ positive sample ($t(40) = -2.44$, $p = 0.019$; Aβ+ mean average error [MAE] = 0.42; Aβ− MAE = 0.79). This suggests that for Aβ positive (but not negative) individuals, the EC-tau burden is closely associated with the degree of MTL excitation by the DMN.

We next used the same approach to test if the excitation of the MTL by the DMN is predictive of the rate of EC-tau accumulation for 32 of the OA who had multiple FTP-PET scans (Table 1). When assessing the out-of-sample performance we observed that estimated values of EC-tau accumulation were significantly associated with the observed values ($r(30) = 0.45$, $p = 0.005$) (Figure 5C). Finally, we stratified the sample by Aβ status (n Aβ+ = 16, n Aβ− = 16) and examined the two samples independently. We observed that the modulation of DMN to MTL connectivity when stimuli are repeated is closely associated with the rate an individual accumulates EC-tau for both Aβ positive and negative groups (Aβ+ $r(14) = 0.51$, $p = 0.021$; Aβ− $r(14) = 0.47$, $p = 0.034$). This suggests that the overall rate an individual is accumulating tau is related to the degree of excitation of the MTL by the DMN and that this relationship may be independent of Aβ status.

Alternative hypotheses

To provide additional support for the cascade of events presented above, we ran a series of LOO analyses testing alternative hypotheses. First, we tested whether the hyperexcitability of the DMN is associated with tau that has migrated out of the EC into the neocortex. We observed no association between tau in regions comprising Braak III/IV stages[37] and the degree of excitation of the DMN by the MTL when stimuli are repeated ($r(40) = 0.07$, $p = 0.33$) (Figure S5A). Second, we tested whether the degree of excitation of the DMN by the MTL drives Aβ accumulation. We observed that the overall rate of Aβ accumulation is not closely linked to the degree of excitation of the DMN by the MTL when stimuli are repeated ($r(30) = 0.25$, $p = 0.082$) (Figure S5B). Third, we tested whether the degree of excitation of the MTL by the DMN is specifically linked to EC-tau accumulation. We observed that the degree of excitation of the MTL by the DMN when stimuli are repeated is not related to the rate of tau accumulation in the inferior temporal lobe ($r(30) = 0.25$, $p = 0.09$) (Figure S5C). Further, we observed that the overall rate of EC-tau accumulation is not related to the degree of excitation of the MTL by the SAL network when stimuli are repeated ($r(30) = 0.13$, $p = 0.24$) (Figure S5D). Together, these additional analyses support the proposal that the hyperexcitation of the DMN reflects the current Aβ burden, which then drives the hyperexcitability of the MTL and the ensuing regionally specific accumulation of tau in the EC.

DISCUSSION

Here, we show the impact of Aβ on E-I balance in a simple repetition suppression task in cognitively normal older people with varying levels of AD pathology. We found that this imbalance was important in determining the deposition and longitudinal accumulation of tau pathology. We observed a transition from the normative inhibitory cortical mechanisms that encode repetition to a pathology-induced excitatory feedback loop. This

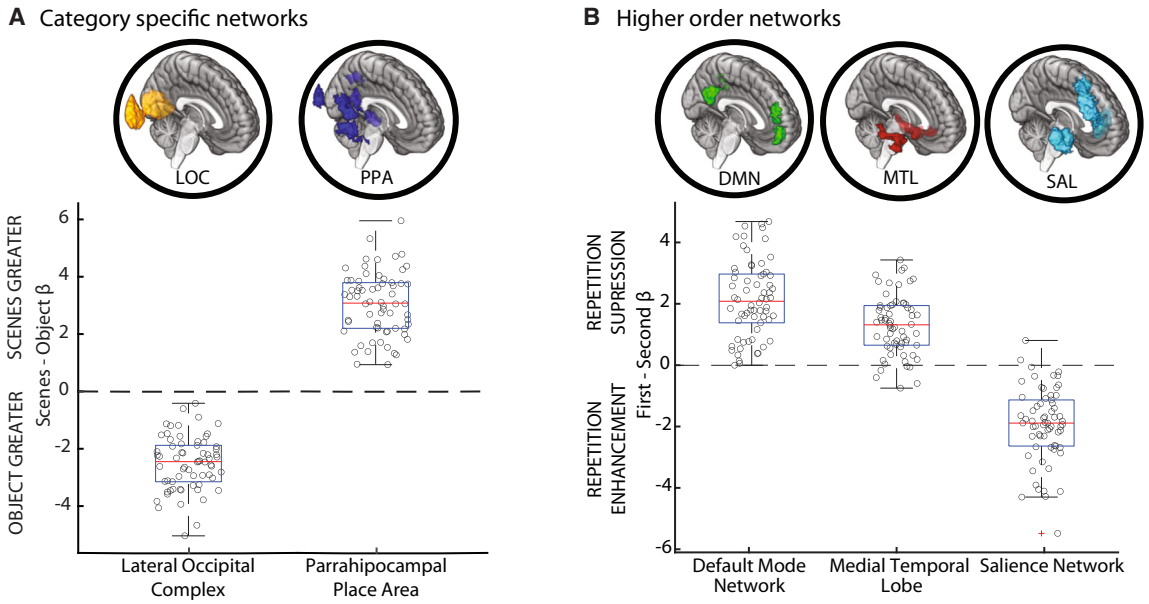

Figure 3. Functional network task activation

(A) Contrast of scenes minus objects activation for the LOC ($t(65) = -21.64$, $p < 0.001$) and PPA ($t(65) = 22.4$, $p < 0.001$), negative values indicate higher activation for objects, positive values represent a higher activation for scenes.

(B) Contrast of novel minus repeated activation for the DMN ($t(65) = 14.04$, $p < 0.001$), MTL ($t(65) = 10.98$, $p < 0.001$) and SAL ($t(65) = -13.14$, $p < 0.001$) networks, positive values show repetition suppression, negative values show repetition enhancement. Dashed line indicates 0 on the y axis. Blue boxes show the 25th and 75th percentile of the data, dashed whiskers show the full range of the data, red lines indicate the median value, and the red cross shows an outlier.

overstimulation of the MTL by the DMN is associated with the rate an individual accumulates tau in the EC.

The ability to effectively implement repetition suppression relies on finely tuned E-I balance and synaptic plasticity, embodied in the sign of the DCM connectivity parameters. Aβ has been shown to impact NMDA glutamate receptors[38] and increase presynaptic glutamate release,[39,40] which, in turn, impairs short-term synaptic plasticity.[41,42] Further, the release of APP leading to Aβ impairs GABAergic interneuron function,[43–45] impacting the passing of signals through the cortical hierarchy.[46] Finally, there are well-established links between dysfunction of the cholinergic system and AD,[47] which will, in turn, impact the fine-scale tuning of cortical responses through gain control.[42,48,49] This disruption to E-I balance has recently been observed in postmortem parietal cortices of early onset AD patients showing elevation in E-I ratios (i.e., hyperexcitability) within brain regions comprising the DMN.[50] Together, this suggests that Aβ and associated cellular functions will have a profound effect on the ability of the local cortical population (i.e., DMN) to undertake efficient processing of repetition through optimal E-I mechanisms. As such, Aβ induced hyperexcitability may underlie the transition of the DMN and MTL from a normative inhibitory loop to an excitatory loop.

The failure of the DMN to "deactivate" during task conditions is well reported for patients with AD.[33,51–53] This transition from normative task-dependent deactivation to activation has also been robustly observed in cognitively normal individuals with Aβ.[54] Similarly, task fMRI paradigms have shown an association between early Braak stage tau and hippocampal hyperactivity.[23,24] Our results indicate that this pattern of hyperactivity is related to E-I imbalance and to the progression of tau pathology, providing evidence that aberrant neural activity may be the crucial process driving remote Aβ and tau interactions.

The accumulation rate of tau in the EC is longitudinally predicted by how much the MTL is excited by the DMN independent of Aβ status, supporting the link between hyperexcitability and tau release shown in mouse models.[13–15] Further, in our analysis of the effects of Aβ on the DMN, we show DMN hyperactivity with increasing levels of Aβ. Given evidence that current Aβ burden is related to the duration of Aβ accumulation,[55] this suggests individuals with a higher Aβ burden may have been in a prolonged period of directed hyperactivity (i.e., MTL over excitation by DMN), resulting in an increased tau burden in EC. We suggest that it is this persistent excitation of the MTL by the DMN when burdened by Aβ that associates Aβ and the primary pathological accumulation of tau in the EC. This provides a plausible mechanistic link between Aβ and EC-tau accumulation through directed hyperactivity, extending work showing associations between MTL activity and tau accumulation observed in a partially overlapping sample.[24]

Our findings can be positioned alongside existing theories that link Aβ and EC-tau accumulation (e.g., the cascading network failure model of AD[56,57]). We find that the association of DMN to MTL hyperactivity and EC-tau deposition falls within the later stages of this model, whereby a compromised DMN "offloads" the burden of processing repeated stimuli onto the MTL where it exacerbates tau accumulation. However, the cascading network failure model posits that DMN hyperconnectivity precedes amyloidosis[58] in the early pathological stages. Here, in contrast, we do not observe a close association between the

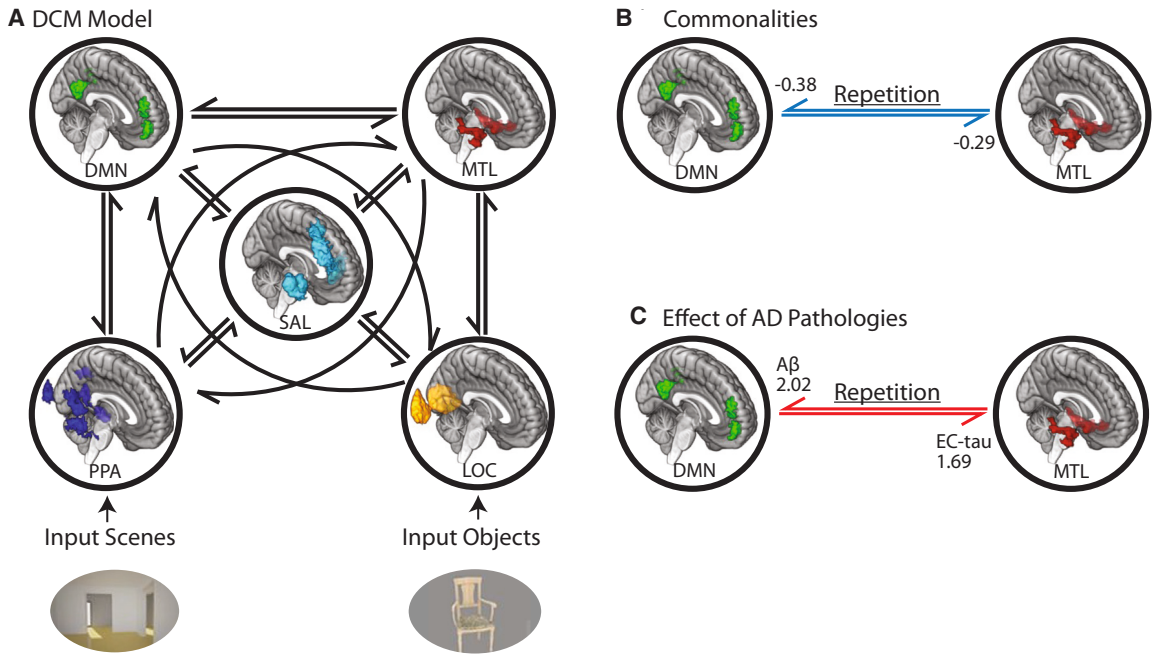

Figure 4. Effects of AD pathology on cortical processing of repetition

(A) DCM model specification. We entered category-specific stimuli into the DCM through input nodes for scenes (PPA) and objects (LOC). We let repetition modulate any connection of a fully connected DCM (except mutual connections between input nodes). Arrows represent the direction of effective connectivity between nodes.

(B and C) Impact of AD pathology on effective connectivity. (B) The commonalties indicating on average the DMN and MTL are inhibited (blue line, negative number) by one another when stimuli are repeated. (C) The effects of colocalized pathology on effective connectivity indicating with greater levels of Aβ the DMN is excited by the MTL (red line, positive number) and with greater levels of EC-tau the MTL is excited by DMN when stimuli are repeated. PEB parameters shown have very strong Bayesian evidence (posterior probability > 0.99).

MTL to DMN hyperactivity and the rate of Aβ accumulation. Previous work has shown connectivity within the DMN follows a nonlinear trajectory, increasing throughout mid-life, plateauing at about 70 years, followed by a subsequent decline.[59] This trajectory of DMN hyperconnectivity tracks with both memory performance[59] and the level of AD pathological burden (i.e., tau in Aβ+ populations).[60] The underlying cause of this trajectory of hyperconnectivity in the DMN is yet to be fully understood and may be in response to the initial presence of Aβ,[61] or, acting in a positive feedback loop with emerging amyloidosis for example through APP processing at the synapse[62] catalyzing cascading network failures.[56,57] It is possible that our sample is at the tipping point of hyperconnectivity in the DMN and thus falls in later stages of Aβ induced changes to network properties.[60,61] However, direct comparison of within-network resting-state connectivity and between-network task-induced hyperactivity is difficult because these variables track distinct neural processes.

The findings presented here also help to explain how Aβ can promote tau propagation despite the disparate spatial patterns of the two pathological proteins. Molecular interactions at a distance or via axonal connectivity have been hypothesized to underlie these events[63]; here, we demonstrate that physiologic factors are crucial. The initial aggregation of Aβ is in the neocortex,[64] and the initial aggregation of cortical tau is in the transentorhinal cortex.[6] As such, early emergence of tau tangles in the entorhinal region occurs in the absence of Aβ plaques in the same location[6,65,66]; therefore, the initial interacting effects of Aβ and tau are likely remote. The long-range hyperexcitation of the MTL by the DMN provides both a biophysically and mechanistically plausible association between regional Aβ and primary pathological tau accumulation in AD.

To test this model, we employed a two-stage computational approach, using high-dimensional ICA to identify DMN and MTL networks, with subsequent hypothesis-driven DCM to infer the interactions between them. Employment of low dimensional ICA often yields a small number of very large networks whereby the hippocampus is embedded in the DMN network.[67] Here, we employed a high-dimensional ICA allowing for a more nuanced view of the task- and disease-dependent dynamic interactions between these more functionally specialized networks. We then infer from the weights of the DCM parameters that these interactions switch from a normative inhibitory effect to excitatory in the presence of AD pathology. Although this approach provides a unique, mechanistic insight into the emergence of AD pathologies, we acknowledge that caution is required when interpretating model-based inferences. Similar to all modeling approaches, DCM rests upon several assumptions, such as the role of low dimensional dynamics shaping population-level neuronal activity.[68]

Our findings should be interpreted in the light of several caveats. Here, we have focused on the transition from normal aging to late-onset sporadic AD, and as such, our findings may not

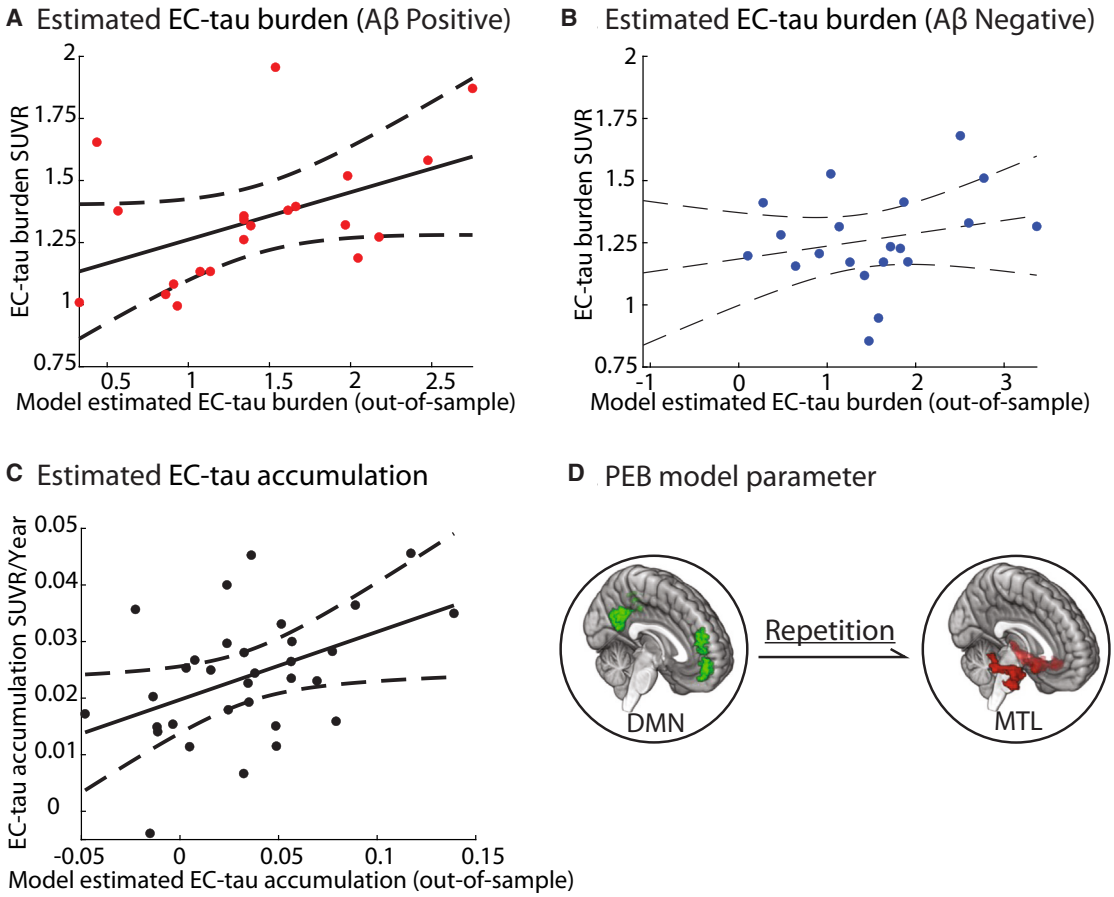

Figure 5. Estimating AD pathology through directed hyperexcitation

(A) Out-of-sample estimation of EC-tau burden for the Aβ positive group ($r(19) = 0.48$, $p = 0.014$).

(B) Out-of-sample estimation of EC-tau burden for the Aβ negative group ($r(19) = 0.20$, $p = 0.2$).

(C) Out-of-sample estimation of the rate of EC-tau accumulation ($r(30) = 0.45$, $p = 0.005$).

(D) PEB parameter used to generate out-of-sample estimates. Out-of-sample predictions of EC-tau burden and accumulation were performed using the degree of excitation of the MTL by the DMN when stimuli are repeated. Group estimates of the relationship of this parameter with EC-tau burden are shown in Figure 4C There was no group level analysis investigating effects of DCM parameters on EC-tau accumulation, rather out-of-sample validation was performed blind when assessing if the degree of excitation of the MTL by the DMN when stimuli are repeated is predictive of the rate of EC-tau accumulation. x axes show estimates of EC-tau burden or accumulation using excitation of MTL by DMN when stimuli are repeated. Mean values were removed from the EC-tau burden or accumulation variables in the PEB models and re-added to both x and y axes for visual purposes.

account for atypical AD cases. Previous work has shown that typical late-onset and atypical variants share disrupted network properties.[69] However, studying these atypical cases longitudinally in asymptomatic stages is difficult due to their uncommon presentations and challenges in early identification.[70] Our analyses focused on how disruptions to cortical processing impacts EC-tau accumulation, a region observed in the vast majority of typical late-onset AD.[1,71,72] Similar to previous accounts related to hyperconnectivity,[69] we conjecture that the core underlying process may be common to these variants, (Aβ-related hyperexcitement → compensatory shift in processing burden → distant tau accumulation) but with a different remote target circuit for the final stage leading to the distinct clinical phenotypes. Further, the task used in this dataset was designed to disassociate cortical memory networks through testing mnemonic discrimination of novel scenes and objects.[34,35] This task context may explain why Aβ-related hyperactivity within the DMN is specific to the afferent stimulation from the MTL, with strong coupling between these regions reported in memory retrieval.[73–79] We suggest the biophysical effects of localized Aβ lead to an increase in the gain of the DMN when receiving these strong task-related afferents,[8–10] which manifests as the hyperexcitability of the DMN that we observe. Future work involving more traditional repetition suppression paradigms that have been shown to elicit robust patterns of parietal connectivity[80,81] may be useful to further investigate if afferent connection from the MTL drives Aβ-related DMN hyperactivity and if this effect extends to other task-specific circuits. Extending beyond repetition suppression, alternative experimental paradigms that probe how the brain processes the regularities of our environment may be employed, such as a probabilistic oddball paradigm.[82,83] These paradigms parametrically assess a more general form of statistical learning—or

predictive coding—which draws on the same mechanisms discussed above (i.e., synaptic plasticity and the E-I balance).[46] This may provide a useful framework to assess the broader range of cognitive and neurological disturbances seen across the AD clinical spectrum.[84] Furthermore, by utilizing brain imaging techniques with a finer timescale (e.g., E/MEG), experimental paradigms could be employed to further probe spectral changes in E-I balance observed in AD.[85]

Conclusions

Our brain processes the overwhelming amount of information bombarding our sensorium through mechanisms such as repetition suppression. These statistical learning mechanisms are constantly performed by the brain and are useful tools to assess how aberrant cortical processing is situated along the AD pathological cascade. We have shown clear disassociations between normative and pathological processing that provides insights into the effect that AD pathologies have on cortical function. In so doing, we propose network-to-network hyperexcitability due to Aβ induced disruptions to E-I balance as a potential causal route that links remote interactions between Aβ and primary tau accumulation.

STAR★METHODS

Detailed methods are provided in the online version of this paper and include the following:

- KEY RESOURCES TABLE
- RESOURCE AVAILABILITY
  - Lead contact
  - Materials availability
  - Data and code availability
- METHOD DETAILS
  - Methods
  - Participants
  - Imaging acquisition and pre-processing
  - Independent Component Analysis (ICA)
  - ICA-GLM
  - Dynamic Causal Modeling (DCM)
  - Parametric Empirical Bayes (PEB)

SUPPLEMENTAL INFORMATION

Supplemental information can be found online at https://doi.org/10.1016/j.neuron.2023.11.014.

ACKNOWLEDGMENTS

Avid Radiopharmaceuticals enabled the use of the 18F-Flortaucipir tracer but did not provide direct funding and were not involved in data analysis or interpretation. J.G. is supported by the Alzheimer's Association (23AARF-1026883). W.J. is supported by the NIH (AG034570 and AG062542). M.B. is supported by NHMRC (APP1152623 and APP2008612).

AUTHOR CONTRIBUTIONS

Conceptualization, J.G., W.J.J., and M.B.; formal analysis, J.G., J.N.A., and A.M.; data curation, J.G., J.N.A, A.M., and W.J.J.; methodology, J.G. and M.B.; writing – original draft, J.G., W.J.J., and M.B.; writing – reviewing & editing, J.G., J.N.A., A.M., W.J.J., and M.B.; supervision W.J.J. and M.B.

DECLARATION OF INTERESTS

W.J. serves as a consultant to Biogen, Genentech, CuraSen, BioClinica, and Novartis.

INCLUSION AND DIVERSITY

We support inclusive, diverse, and equitable conduct of research.

Received: March 24, 2023
Revised: September 1, 2023
Accepted: November 14, 2023
Published: December 13, 2023

REFERENCES

1. Jagust, W. (2018). Imaging the evolution and pathophysiology of Alzheimer disease. Nat. Rev. Neurosci. *19*, 687–700.
2. Villeneuve, S., Rabinovici, G.D., Cohn-Sheehy, B.I., Madison, C., Ayakta, N., Ghosh, P.M., La Joie, R., Arthur-Bentil, S.K., Vogel, J.W., Marks, S.M., et al. (2015). Existing Pittsburgh compound-B positron emission tomography thresholds are too high: statistical and pathological evaluation. Brain *138*, 2020–2033.
3. Palmqvist, S., Schöll, M., Strandberg, O., Mattsson, N., Stomrud, E., Zetterberg, H., Blennow, K., Landau, S., Jagust, W., and Hansson, O. (2017). Earliest accumulation of β-amyloid occurs within the default-mode network and concurrently affects brain connectivity. Nat. Commun. *8*, 1214.
4. Bennett, R.E., DeVos, S.L., Dujardin, S., Corjuc, B., Gor, R., Gonzalez, J., Roe, A.D., Frosch, M.P., Pitstick, R., Carlson, G.A., et al. (2017). Enhanced tau aggregation in the presence of amyloid β. Am. J. Pathol. *187*, 1601–1612.
5. Pontecorvo, M.J., Devous, M.D., Navitsky, M., Lu, M., Salloway, S., Schaerf, F.W., Jennings, D., Arora, A.K., McGeehan, A., Lim, N.C., et al. (2017). Relationships between flortaucipir PET tau binding and amyloid burden, clinical diagnosis, age and cognition. Brain *140*, 748–763.
6. Braak, H., and Braak, E. (1991). Neuropathological stageing of Alzheimer-related changes. Acta Neuropathol. *82*, 239–259.
7. Jack, C.R., Knopman, D.S., Jagust, W.J., Shaw, L.M., Aisen, P.S., Weiner, M.W., Petersen, R.C., and Trojanowski, J.Q. (2010). Hypothetical model of dynamic biomarkers of the Alzheimer's pathological cascade. Lancet Neurol. *9*, 119–128.
8. Busche, M.A., and Konnerth, A. (2016). Impairments of neural circuit function in Alzheimer's disease. Philos. Trans. R. Soc. Lond. B Biol. Sci. *371*, 20150429.
9. Palop, J.J., and Mucke, L. (2016). Network abnormalities and interneuron dysfunction in Alzheimer disease. Nat. Rev. Neurosci. *17*, 777–792.
10. Harris, S.S., Wolf, F., De Strooper, B., and Busche, M.A. (2020). Tipping the scales: peptide-dependent dysregulation of neural circuit dynamics in Alzheimer's disease. Neuron *107*, 417–435.
11. Villemagne, V.L., Burnham, S., Bourgeat, P., Brown, B., Ellis, K.A., Salvado, O., Szoeke, C., Macaulay, S.L., Martins, R., Maruff, P., et al. (2013). Amyloid β deposition, neurodegeneration, and cognitive decline in sporadic Alzheimer's disease: a prospective cohort study. Lancet Neurol. *12*, 357–367.
12. Hanseeuw, B.J., Betensky, R.A., Jacobs, H.I.L., Schultz, A.P., Sepulcre, J., Becker, J.A., Cosio, D.M.O., Farrell, M., Quiroz, Y.T., Mormino, E.C., et al. (2019). Association of amyloid and tau with cognition in preclinical Alzheimer disease: a longitudinal study. JAMA Neurol. *76*, 915–924.
13. Wu, J.W., Hussaini, S.A., Bastille, I.M., Rodriguez, G.A., Mrejeru, A., Rilett, K., Sanders, D.W., Cook, C., Fu, H., Boonen, R.A.C.M., et al. (2016). Neuronal activity enhances tau propagation and tau pathology in vivo. Nat. Neurosci. *19*, 1085–1092.

14. Pooler, A.M., Phillips, E.C., Lau, D.H.W., Noble, W., and Hanger, D.P. (2013). Physiological release of endogenous tau is stimulated by neuronal activity. EMBO Rep. *14*, 389–394.

15. Yamada, K., Holth, J.K., Liao, F., Stewart, F.R., Mahan, T.E., Jiang, H., Cirrito, J.R., Patel, T.K., Hochgräfe, K., Mandelkow, E.M., et al. (2014). Neuronal activity regulates extracellular tau in vivo. J. Exp. Med. *211*, 387–393.

16. Billette, O.V., Ziegler, G., Aruci, M., Schütze, H., Kizilirmak, J.M., Richter, A., Altenstein, S., Bartels, C., Brosseron, F., Cardenas-Blanco, A., et al. (2022). Novelty-related fMRI responses of precuneus and medial temporal regions in individuals at risk for Alzheimer disease. Neurology *99*, e775–e788.

17. Corriveau-Lecavalier, N., Mellah, S., Clément, F., and Belleville, S. (2019). Evidence of parietal hyperactivation in individuals with mild cognitive impairment who progressed to dementia: a longitudinal fMRI study. NeuroImage Clin. *24*, 101958.

18. Sperling, R., Mormino, E., and Johnson, K. (2014). The evolution of preclinical Alzheimer's disease: implications for prevention trials. Neuron *84*, 608–622.

19. Berron, D., Cardenas-Blanco, A., Bittner, D., Metzger, C.D., Spottke, A., Heneka, M.T., Fliessbach, K., Schneider, A., Teipel, S.J., Wagner, M., et al. (2019). Higher CSF tau levels are related to hippocampal hyperactivity and object mnemonic discrimination in older adults. J. Neurosci. *39*, 8788–8797.

20. Yassa, M.A., Lacy, J.W., Stark, S.M., Albert, M.S., Gallagher, M., and Stark, C.E.L. (2011). Pattern separation deficits associated with increased hippocampal CA3 and dentate gyrus activity in nondemented older adults. Hippocampus *21*, 968–979.

21. Reagh, Z.M., Noche, J.A., Tustison, N.J., Delisle, D., Murray, E.A., and Yassa, M.A. (2018). Functional imbalance of anterolateral entorhinal cortex and hippocampal dentate/CA3 underlies age-related object pattern separation deficits. Neuron *97*, 1187–1198.e4.

22. Huijbers, W., Schultz, A.P., Papp, K.V., LaPoint, M.R., Hanseeuw, B., Chhatwal, J.P., Hedden, T., Johnson, K.A., and Sperling, R.A. (2019). Tau accumulation in clinically normal older adults is associated with hippocampal hyperactivity. J. Neurosci. *39*, 548–556.

23. Marks, S.M., Lockhart, S.N., Baker, S.L., and Jagust, W.J. (2017). Tau and β-amyloid are associated with medial temporal lobe structure, function, and memory encoding in normal aging. J. Neurosci. *37*, 3192–3201.

24. Adams, J.N., Harrison, T.M., Maass, A., Baker, S.L., and Jagust, W.J. (2022). Distinct factors drive the spatiotemporal progression of tau pathology in older adults. J. Neurosci. *42*, 1352–1361.

25. Gross, C.G., Bender, D.B., and Rocha-Miranda, C.E. (1969). Visual receptive fields of neurons in inferotemporal cortex of the monkey. Science *166*, 1303–1306.

26. Miller, E.K., and Desimone, R. (1994). Parallel neuronal mechanisms for short-term memory. Science *263*, 520–522.

27. Miller, E.K., Li, L., and Desimone, R. (1991). A neural mechanism for working and recognition memory in inferior temporal cortex. Science *254*, 1377–1379.

28. Knill, D.C., and Pouget, A. (2004). The Bayesian brain: the role of uncertainty in neural coding and computation. Trends Neurosci. *27*, 712–719.

29. Gregory, R.L. (1980). Perceptions as hypotheses. Philos. Trans. R. Soc. Lond. B Biol. Sci. *290*, 181–197.

30. Adams, J.N., Maass, A., Berron, D., Harrison, T.M., Baker, S.L., Thomas, W.P., Stanfill, M., and Jagust, W.J. (2021). Reduced repetition suppression in aging is driven by tau-related hyperactivity in medial temporal lobe. J. Neurosci. *41*, 3917–3931.

31. Jurick, S.M., Weissberger, G.H., Clark, L.R., Wierenga, C.E., Chang, Y.L., Schiehser, D.M., Han, S.D., Jak, A.J., Dev, S.I., and Bondi, M.W. (2018). Faulty adaptation to repeated face-name associative pairs in mild cognitive impairment is predictive of cognitive decline. Arch. Clin. Neuropsychol. *33*, 168–183.

32. Pihlajamäki, M., O'Keefe, K., O'Brien, J., Blacker, D., and Sperling, R.A. (2011). Failure of repetition suppression and memory encoding in aging and Alzheimer's disease. Brain Imaging Behav. *5*, 36–44.

33. Pihlajamäki, M., Depeau, K.M., Blacker, D., and Sperling, R.A. (2008). Impaired medial temporal repetition suppression is related to failure of parietal deactivation in Alzheimer disease. Am. J. Geriatr. Psychiatry *16*, 283–292.

34. Maass, A., Berron, D., Harrison, T.M., Adams, J.N., La Joie, R., Baker, S., Mellinger, T., Bell, R.K., Swinnerton, K., Inglis, B., et al. (2019). Alzheimer's pathology targets distinct memory networks in the ageing brain. Brain *142*, 2492–2509.

35. Berron, D., Neumann, K., Maass, A., Schütze, H., Fliessbach, K., Kiven, V., Jessen, F., Sauvage, M., Kumaran, D., and Düzel, E. (2018). Age-related functional changes in domain-specific medial temporal lobe pathways. Neurobiol. Aging *65*, 86–97.

36. Rissanen, J. (1978). Modeling by shortest data description. Automatica *14*, 465–471.

37. Maass, A., Landau, S., Baker, S.L., Horng, A., Lockhart, S.N., La Joie, R., Rabinovici, G.D., and Jagust, W.J.; Alzheimer's Disease Neuroimaging Initiative (2017). Comparison of multiple tau-PET measures as biomarkers in aging and Alzheimer's disease. Neuroimage *157*, 448–463.

38. Um, J.W., Nygaard, H.B., Heiss, J.K., Kostylev, M.A., Stagi, M., Vortmeyer, A., Wisniewski, T., Gunther, E.C., and Strittmatter, S.M. (2012). Alzheimer amyloid-β oligomer bound to postsynaptic prion protein activates Fyn to impair neurons. Nat. Neurosci. *15*, 1227–1235.

39. Hascup, K.N., and Hascup, E.R. (2015). Altered neurotransmission prior to cognitive decline in AβPP/PS1 mice, a model of Alzheimer's disease. J. Alzheimers Dis. *44*, 771–776.

40. Jin, N., Gureviciene, I., Atalay, A.N., Häkli, S., Ziyatdinova, S., and Tanila, H. (2022). Preclinical evaluation of drug treatment options for sleep-related epileptiform spiking in Alzheimer's disease. Alzheimers. Dement. (N Y) *8*, e12291.

41. Schmidt, A., Diaconescu, A.O., Kometer, M., Friston, K.J., Stephan, K.E., and Vollenweider, F.X. (2013). Modeling ketamine effects on synaptic plasticity during the mismatch negativity. Cereb. Cortex *23*, 2394–2406.

42. Auksztulewicz, R., and Friston, K. (2016). Repetition suppression and its contextual determinants in predictive coding. Cortex *80*, 125–140.

43. Busche, M.A., Eichhoff, G., Adelsberger, H., Abramowski, D., Wiederhold, K.H., Haass, C., Staufenbiel, M., Konnerth, A., and Garaschuk, O. (2008). Clusters of hyperactive neurons near amyloid plaques in a mouse model of Alzheimer's disease. Science *321*, 1686–1689.

44. Kim, D.Y., Carey, B.W., Wang, H., Ingano, L.A.M., Binshtok, A.M., Wertz, M.H., Pettingell, W.H., He, P., Lee, V.M.Y., Woolf, C.J., et al. (2007). BACE1 regulates voltage-gated sodium channels and neuronal activity. Nat. Cell Biol. *9*, 755–764.

45. Verret, L., Mann, E.O., Hang, G.B., Barth, A.M.I., Cobos, I., Ho, K., Devidze, N., Masliah, E., Kreitzer, A.C., Mody, I., et al. (2012). Inhibitory interneuron deficit links altered network activity and cognitive dysfunction in alzheimer model. Cell *149*, 708–721.

46. Bastos, A.M., Usrey, W.M., Adams, R.A., Mangun, G.R., Fries, P., and Friston, K.J. (2012). Canonical microcircuits for predictive coding. Neuron *76*, 695–711.

47. Buckingham, S.D., Jones, A.K., Brown, L.A., and Sattelle, D.B. (2009). Nicotinic acetylcholine receptor signalling: roles in Alzheimer's disease and amyloid neuroprotection. Pharmacol. Rev. *61*, 39–61.

48. Baldeweg, T., Wong, D., and Stephan, K.E. (2006). Nicotinic modulation of human auditory sensory memory: evidence from mismatch negativity potentials. Int. J. Psychophysiol. *59*, 49–58.

49. Moran, R.J., Campo, P., Symmonds, M., Stephan, K.E., Dolan, R.J., and Friston, K.J. (2013). Free energy, precision and learning: the role of cholinergic neuromodulation. J. Neurosci. *33*, 8227–8236.

50. Lauterborn, J.C., Scaduto, P., Cox, C.D., Schulmann, A., Lynch, G., Gall, C.M., Keene, C.D., and Limon, A. (2021). Increased excitatory to inhibitory

synaptic ratio in parietal cortex samples from individuals with Alzheimer's disease. Nat. Commun. *12*, 2603.

51. Mevel, K., Chételat, G., Eustache, F., and Desgranges, B. (2011). The default mode network in healthy aging and Alzheimer's disease. Int. J. Alzheimers Dis. *2011*, 535816.
52. Hafkemeijer, A., van der Grond, J., and Rombouts, S.A.R.B. (2012). Imaging the default mode network in aging and dementia. Biochim. Biophys. Acta *1822*, 431–441.
53. Lustig, C., Snyder, A.Z., Bhakta, M., O'Brien, K.C., McAvoy, M., Raichle, M.E., Morris, J.C., and Buckner, R.L. (2003). Functional deactivations: change with age and dementia of the Alzheimer type. Proc. Natl. Acad. Sci. USA *100*, 14504–14509.
54. Sperling, R.A., LaViolette, P.S., O'Keefe, K., O'Brien, J., Rentz, D.M., Pihlajamaki, M., Marshall, G., Hyman, B.T., Selkoe, D.J., Hedden, T., et al. (2009). Amyloid deposition is associated with impaired default network function in older persons without dementia. Neuron *63*, 178–188.
55. Schindler, S.E., Li, Y., Buckles, V.D., Gordon, B.A., Benzinger, T.L.S., Wang, G., Coble, D., Klunk, W.E., Fagan, A.M., Holtzman, D.M., et al. (2021). Predicting symptom onset in sporadic Alzheimer disease with amyloid PET. Neurology *97*, e1823–e1834.
56. Jones, D.T., Knopman, D.S., Gunter, J.L., Graff-Radford, J., Vemuri, P., Boeve, B.F., Petersen, R.C., Weiner, M.W., and Jack, C.R.; Alzheimer's Disease Neuroimaging Initiative (2016). Cascading network failure across the Alzheimer's disease spectrum. Brain *139*, 547–562.
57. Jones, D.T., Graff-Radford, J., Lowe, V.J., Wiste, H.J., Gunter, J.L., Senjem, M.L., Botha, H., Kantarci, K., Boeve, B.F., Knopman, D.S., et al. (2017). Tau, amyloid, and cascading network failure across the Alzheimer's disease spectrum. Cortex *97*, 143–159.
58. Jack, C.R., Wiste, H.J., Weigand, S.D., Knopman, D.S., Lowe, V., Vemuri, P., Mielke, M.M., Jones, D.T., Senjem, M.L., Gunter, J.L., et al. (2013). Amyloid-first and neurodegeneration-first profiles characterize incident amyloid PET positivity. Neurology *81*, 1732–1740.
59. Staffaroni, A.M., Brown, J.A., Casaletto, K.B., Elahi, F.M., Deng, J., Neuhaus, J., Cobigo, Y., Mumford, P.S., Walters, S., Saloner, R., et al. (2018). The longitudinal trajectory of default mode network connectivity in healthy older adults varies as a function of age and is associated with changes in episodic memory and processing speed. J. Neurosci. *38*, 2809–2817.
60. Schultz, A.P., Chhatwal, J.P., Hedden, T., Mormino, E.C., Hanseeuw, B.J., Sepulcre, J., Huijbers, W., LaPoint, M., Buckley, R.F., Johnson, K.A., et al. (2017). Phases of hyperconnectivity and hypoconnectivity in the default mode and salience networks track with amyloid and tau in clinically normal individuals. J. Neurosci. *37*, 4323–4331.
61. Hillary, F.G., and Grafman, J.H. (2017). Injured brains and adaptive networks: the benefits and costs of hyperconnectivity. Trends Cogn. Sci. *21*, 385–401.
62. Busche, M.A., and Konnerth, A. (2015). Neuronal hyperactivity – a key defect in Alzheimer's disease? BioEssays *37*, 624–632.
63. Lee, W.J., Brown, J.A., Kim, H.R., La Joie, R., Cho, H., Lyoo, C.H., Rabinovici, G.D., Seong, J.-K., and Seeley, W.W.; Alzheimer's Disease Neuroimaging Initiative (2022). Regional Aβ-tau interactions promote onset and acceleration of Alzheimer's disease tau spreading. Neuron *110*, 1932–1943.e5.
64. Thal, D.R., Rüb, U., Orantes, M., and Braak, H. (2002). Phases of Aβ-deposition in the human brain and its relevance for the development of AD. Neurology *58*, 1791–1800.
65. Price, J.L., Davis, P.B., Morris, J.C., and White, D.L. (1991). The distribution of tangles, plaques and related immunohistochemical markers in healthy aging and Alzheimer's disease. Neurobiol. Aging *12*, 295–312.
66. Schönheit, B., Zarski, R., and Ohm, T.G. (2004). Spatial and temporal relationships between plaques and tangles in Alzheimer-pathology. Neurobiol. Aging *25*, 697–711.
67. Damoiseaux, J.S., Rombouts, S.A.R.B., Barkhof, F., Scheltens, P., Stam, C.J., Smith, S.M., and Beckmann, C.F. (2006). Consistent resting-state networks across healthy subjects. Proc. Natl. Acad. Sci. USA *103*, 13848–13853.
68. Breakspear, M. (2017). Dynamic models of large-scale brain activity. Nat. Neurosci. *20*, 340–352.
69. Corriveau-Lecavalier, N., Gunter, J.L., Kamykowski, M., Dicks, E., Botha, H., Kremers, W.K., Graff-Radford, J., Wiepert, D.A., Schwarz, C.G., Yacoub, E., et al. (2023). Default mode network failure and neurodegeneration across aging and amnestic and dysexecutive Alzheimer's disease. Brain Commun. *5*, fcad058.
70. Graff-Radford, J., Yong, K.X.X., Apostolova, L.G., Bouwman, F.H., Carrillo, M., Dickerson, B.C., Rabinovici, G.D., Schott, J.M., Jones, D.T., and Murray, M.E. (2021). New insights into atypical Alzheimer's disease in the era of biomarkers. Lancet Neurol. *20*, 222–234.
71. Young, C.B., Winer, J.R., Younes, K., Cody, K.A., Betthauser, T.J., Johnson, S.C., Schultz, A., Sperling, R.A., Greicius, M.D., Cobos, I., et al. (2022). Divergent cortical tau positron emission tomography patterns among patients with preclinical Alzheimer disease. JAMA Neurol. *79*, 592–603.
72. Sanchez, J.S., Becker, J.A., Jacobs, H.I.L., Hanseeuw, B.J., Jiang, S., Schultz, A.P., Properzi, M.J., Katz, S.R., Beiser, A., Satizabal, C.L., et al. (2021). The cortical origin and initial spread of medial temporal tauopathy in Alzheimer's disease assessed with positron emission tomography. Sci. Transl. Med. *13*, 655.
73. Ranganath, C., Heller, A., Cohen, M.X., Brozinsky, C.J., and Rissman, J. (2005). Functional connectivity with the hippocampus during successful memory formation. Hippocampus *15*, 997–1005.
74. Ranganath, C., and Ritchey, M. (2012). Two cortical systems for memory-guided behaviour. Nat. Rev. Neurosci. *13*, 713–726.
75. Jeong, W., Chung, C.K., and Kim, J.S. (2015). Episodic memory in aspects of large-scale brain networks. Front. Hum. Neurosci. *9*, 454.
76. Spaniol, J., Davidson, P.S.R., Kim, A.S.N., Han, H., Moscovitch, M., and Grady, C.L. (2009). Event-related fMRI studies of episodic encoding and retrieval: meta-analyses using activation likelihood estimation. Neuropsychologia *47*, 1765–1779.
77. Chrastil, E.R. (2018). Heterogeneity in human retrosplenial cortex: a review of function and connectivity. Behav. Neurosci. *132*, 317–338.
78. Li, X., Kehoe, E.G., Mcginnity, T.M., Coyle, D., and Bokde, A.L.W. (2015). Modulation of effective connectivity in the default mode network at rest and during a memory task. Brain Connect. *5*, 60–67.
79. Huijbers, W., Pennartz, C.M.A., Cabeza, R., and Daselaar, S.M. (2011). The hippocampus is coupled with the default network during memory retrieval but not during memory encoding. PLoS One *6*, e17463.
80. Zamboni, E., Kemper, V.G., Goncalves, N.R., Jia, K., Karlaftis, V.M., Bell, S.J., Giorgio, J., Rideaux, R., Goebel, R., and Kourtzi, Z. (2020). Fine-scale computations for adaptive processing in the human brain. eLife *9*, e57637.
81. Karlaftis, V.M., Giorgio, J., Zamboni, E., Frangou, P., Rideaux, R., Ziminski, J.J., and Kourtzi, Z. (2021). Functional interactions between sensory and memory networks for adaptive behavior. Cereb. Cortex *31*, 5319–5330.
82. Lieder, F., Stephan, K.E., Daunizeau, J., Garrido, M.I., and Friston, K.J. (2013). A neurocomputational model of the mismatch negativity. PLoS Comput. Biol. *9*, e1003288.
83. Garrido, M.I., Sahani, M., and Dolan, R.J. (2013). Outlier responses reflect sensitivity to statistical structure in the human brain. PLoS Comput. Biol. *9*, e1002999.
84. Kocagoncu, E., Klimovich-Gray, A., Hughes, L.E., and Rowe, J.B. (2021). Evidence and implications of abnormal predictive coding in dementia. Brain *144*, 3311–3321.
85. Ranasinghe, K.G., Verma, P., Cai, C., Xie, X., Kudo, K., Gao, X., Lerner, H., Mizuiri, D., Strom, A., Iaccarino, L., et al. (2022). Altered excitatory and inhibitory neuronal subpopulation parameters are distinctly associated with tau and amyloid in Alzheimer's disease. eLife *11*, e77850.

86. Harrison, T.M., La Joie, R., Maass, A., Baker, S.L., Swinnerton, K., Fenton, L., Mellinger, T.J., Edwards, L., Pham, J., Miller, B.L., et al. (2019). Longitudinal tau accumulation and atrophy in aging and Alzheimer disease. Ann. Neurol. *85*, 229–240.

87. Rousset, O.G., Ma, Y., and Evans, A.C. (1998). Correction for partial volume effects in PET: principle and validation. J. Nucl. Med. *39*, 904–911.

88. Baker, S.L., Maass, A., and Jagust, W.J. (2017). Considerations and code for partial volume correcting [18F]-AV-1451 tau PET data. Data Brief *15*, 648–657.

89. Chen, Z., and Calhoun, V. (2018). Effect of spatial smoothing on task fMRI ICA and functional connectivity. Front. Neurosci. *12*, 15.

90. Power, J.D., Schlaggar, B.L., and Petersen, S.E. (2015). Recent progress and outstanding issues in motion correction in resting state fMRI. Neuroimage *105*, 536–551.

91. Zeidman, P., Jafarian, A., Corbin, N., Seghier, M.L., Razi, A., Price, C.J., and Friston, K.J. (2019). A guide to group effective connectivity analysis, part 1: first level analysis with DCM for fMRI. Neuroimage *200*, 174–190.

92. Friston, K.J., Harrison, L., and Penny, W. (2003). Dynamic causal modelling. Neuroimage *19*, 1273–1302.

93. Daunizeau, J., David, O., and Stephan, K.E. (2011). Dynamic causal modelling: a critical review of the biophysical and statistical foundations. Neuroimage *58*, 312–322.

94. Zeidman, P., Jafarian, A., Seghier, M.L., Litvak, V., Cagnan, H., Price, C.J., and Friston, K.J. (2019). A guide to group effective connectivity analysis, part 2: second level analysis with PEB. Neuroimage *200*, 12–25.

95. Friston, K.J., Litvak, V., Oswal, A., Razi, A., Stephan, K.E., Van Wijk, B.C.M., Ziegler, G., and Zeidman, P. (2016). Bayesian model reduction and empirical Bayes for group (DCM) studies. Neuroimage *128*, 413–431.

96. Friston, K.J., Preller, K.H., Mathys, C., Cagnan, H., Heinzle, J., Razi, A., and Zeidman, P. (2019). Dynamic causal modelling revisited. Neuroimage *199*, 730–744.

STAR★METHODS

KEY RESOURCES TABLE

REAGENT or RESOURCE	SOURCE	IDENTIFIER
Software and algorithms		
MATLAB	Mathworks	https://www.mathworks.com
SPM	The Wellcome Centre For Human Neuroimaging	https://www.fil.ion.ucl.ac.uk/spm/
GIFT	Translational Research in Neuroimaging & Data Science	https://trendscenter.org/software/gift/
FreeSurfer	Open source	http://surfer.nmr.mgh.harvard.edu/

RESOURCE AVAILABILITY

Lead contact

Further information and requests for resources should be directed to and will be fulfilled by the lead contact, Joseph Giorgio (jgiorgio@berkeley.edu).

Materials availability

Data associated with this work are raw neuroimaging files that are not publicly available. For access to this data material transfer agreements between research institutions are required.

Data and code availability

No original code was developed for this work. The application of DCM and PEB was executed in SPM12.

METHOD DETAILS

Methods

72 participants (50 cognitively normal OA, 22 YA) performed an fMRI task involving novel and repeated scenes and objects. 42 of these OA had measures of both Aβ using PiB-PET and cross-sectional EC-tau using FTP-PET. We decomposed the fMRI data for 66 participants (45 OA, 21YA) who passed quality control into functional networks using group spatial ICA and then used DCM to infer cortical interactions supporting responses to repeated stimuli. We used a hierarchical Bayesian approach to uncover how individual differences in these interactions are related to AD pathologies. Finally, we ran leave one out validation to use these network interactions to estimate cross sectional and longitudinal EC-tau.

Participants

Cognitively normal OA and YA were recruited as part of the Berkeley Aging Cohort Study. OA are community-dwelling cognitively normal elderly individuals with a Geriatric depression scale (GDS) score $\leq$10, Mini mental status examination (MMSE) score $\geq$25, no current neurological and psychiatric illness, normal functions on verbal and visual memory tests (all scores ≥ -1.5 SD of age-adjusted, gender-adjusted, and education-adjusted norms) and age 60–90 (inclusive) years. The Institutional Review Boards of the University of California, Berkeley and the Lawrence Berkeley National Laboratory (LBNL) approved this study. All participants provided written informed consent.

Imaging acquisition and pre-processing

Imaging acquisition, participant exclusion, task design and pre-processing have also been described elsewhere.[30]

PET imaging

42 of the OA underwent molecular imaging on a Siemens Biograph PET/CT to measure both global Aβ and EC-tau burden. For Aβ imaging ~15 mCi if PiB tracer was injected into an antecubital vein, and dynamic acquisition frames were obtained over a 90 min measurement interval (4 × 15 s frames, 8 × 30 s frames, 9 × 60 s frames, 2 × 180 s frames, 8 × 300 s frames, and 3 × 600 s frames) following an X-ray CT. Distribution volume ratios (DVRs) were generated with Logan graphical analysis on the aligned PiB frames using the native-space grey matter cerebellum as a reference region. PiB images were fit in the 35–90 min window following injection. For each subject, a global cortical PiB index was derived from the native-space DVR image coregistered to the MRI using FreeSurfer (5.3) parcellations using the Desikan–Killiany atlas to define frontal (cortical regions anterior to the precentral sulcus), temporal

(middle and superior temporal regions), parietal (supramarginal gyrus, inferior/superior parietal lobules, and precuneus), and anterior/posterior cingulate regions- ROIs combined as a weighted average. There was no partial volume correction performed. To assign Aβ positivity a threshold of DVR>1.065 was used. To extract rates of subject specific Aβ accumulation we used linear mixed-effects-models.[24,86]

The FTP-PET protocol entailed the injection of 10 mCi of tracer followed by acquisition 80–100 min post injection. FTP data were realigned and the mean of all frames used to co-register FTP to each participant's MRI acquired closest to the time of the FTP-PET. Standardized uptake value ratio (SUVR) images were calculated by averaging mean tracer uptake over the 80- to 100-min data normalized by an inferior cerebellar grey reference region. The mean SUVR of each native space FreeSurfer ROI was extracted and partial volume corrected using a modified Geometric Transfer Matrix approach.[87,88] We used partial volume corrected data to ensure that off-target FTP signal and partial volume effects did not affect measures of FTP in the entorhinal ROI. We carried forward the averaged SUVR value for left and right entorhinal ROIs from the Desikan-Killiany atlas as our measure of cross sectional EC-tau. To extract regional rates of tau accumulation we used a previously published processing pipeline involving an optimised white matter reference region to derive SUVRs and linear mixed-effects-models to extract subject and region specific rates of accumulation.[24,86]

fMRI acquisition

3T acquisition of structural and functional MRI was performed at the Henry H. Wheeler Jr. Brain Imaging Centre with a 3T TIM/Trio scanner (Siemens Medical system, software version B17A) and a 32-channel head coil. Whole brain structural images were acquired using a T1-weighted volumetric magnetization prepared rapid gradient echo image (MPRAGE; voxel size = 1 mm isotropic, TR = 2300 ms, TE = 2.98 ms, matrix = 256 240 160, FOV = 256 240 160 mm3, sagittal plane, 160 slices, 5-min acquisition time). High-resolution whole-brain functional data were acquired using T2*-weighted gradientecho echoplanar images (GE-EPI; voxel size = 1.54 mm isotropic, multiband acceleration factor 4, TR = 2400 ms, TE = 37 ms, flip angle = 45, matrix = 138 138, FoV = 212 212 mm2, interleaved acquisition, 88 slices, PA phase encoding, two 13 min runs). Two gradient echo images with different echo times were additionally collected for distortion correction (1.54-mm isotropic resolution, R-L encoding direction, TR = 1000 ms, flip angle = 60, TE1 = 5.6 ms, TE2 = 8.06 ms).

Task

fMRI was acquired while participants were presented with blocks of four stimuli of either objects or scenes with the first two stimuli within a block novel and the next two stimuli either the same or a similar lure stimulus. Throughout the task participants were instructed to indicate whether a stimulus was old or new. Within the scanning session, participants performed two runs of the task comprising 128 trials (64 first-repeat pairs, 64 first-lure pairs). Each run began and ended with a perceptual baseline condition, which consisted of scrambled noise images with similar luminosity and colour to the test stimuli. Stimuli were presented in an event-related design using Neurobehavioral Systems (https://nbs.neurobs.com). Each object or scene image was shown for 3 s and separated by a white fixation star with jittered interstimulus intervals ranging from 0.6 to 4.2 s. Prior to the scanning sessions participants were trained on the task to ensure familiarity and excluded if performance on the mnemonic discrimination in the scanner was close to chance (n=3 OA).[34]

fMRI preprocessing

fMRI preprocessing was conducted with Statistical Parametric Mapping (SPM, version 12, Wellcome Trust Center for Neuroimaging, London, United Kingdom). The first five images of each fMRI run were discarded to ensure T1 equilibrium. Slice time correction was performed to correct for differences in acquisition, using the middle slice in time as a reference. Motion and distortion correction was then performed using the FieldMap toolbox v2.1 with the "realign and unwarp" SPM module. During this process, the T1 image was coregistered to the first EPI, and all EPIs were realigned to the first EPI image. EPIs were spatially smoothed with a 4mm Gaussian kernel to improve the group estimation of spatial independent components.[89] Outlier frames for each run were included as spike regressors in the first-level design matrix.[90] Outliers were detected based on average intensity (z-score of 5) and motion (0.9 mm/TR) using the art.m function of the CONN toolbox, with participants excluded if 20% of the fMRI volumes we detected as outliers (n= 2 OA; 1 YA).

Independent Component Analysis (ICA)

We used spatial group ICA to extract participant specific hemodynamic source locations using the Group ICA fMRI Toolbox (GIFT) (http://mialab.mrn.org/software/gift/). Pre-processed fMRI data from both groups (i.e. YA and OA) were included in the group ICA to get a robust estimation of the task based cortical networks of interest. We used the Minimum Description Length criteria[36] to estimate the dimensionality and determine the number of independent components for dimensionality reduction. We used a two-level dimensionality reduction procedure using Principal Component Analysis; first at the participant level and then at the group level. The ICA estimation (Infomax algorithm) was run 20 times and the component stability was estimated using ICASSO. This procedure resulted in 67 spatially independent components. For each subject we generated participant-specific spatial maps for each component using back reconstruction. The result of the ICA is a time course for each component (functional network) for each participant while they performed the task. To ensure that all time courses are in a comparable range across subjects we normalized each component time course for each run to have a mean of 0 and a standard deviation of 1 (i.e. z-score). Finally, we ran a one sample t-test on these back reconstructed spatial maps to estimate a group level spatial map and determine which cortical voxels are significant hemodynamic sources within each component. To ensure the ICA time series for our networks of interest were not subject to any unaccounted-for axis rotations we correlated the average and ICA timeseries. Within the DMN and MTL we observed no unaccounted flipping in the

sign of the time series in the ICA estimation (average signal vs. ICA signal (Pearson's correlation coefficient, DMN mean±std (r=0.37±0.14), t(65)=21.7, p<0.001; MTL mean±std (r=0.42±0.16), t(65)=21.0, p<0.001)).

ICA-GLM

To assess the task related activity for these ICA-derived cortical networks, we regressed the normalized time courses against the task design. We extracted parameter weights (β-weights) for stimulus category (i.e. object or scene) as well as novel and repeated stimuli. The GLM included as confounds of no interest spike regressors for outlier frames as well as the 6 motion parameters estimated in realignment. We assessed the cortical activity in response to stimulus category (i.e. objects β-weight – scenes β-weight) and repetition (novel β-weight – repeated β-weight) for each of our cortical networks using one sample t-tests against 0 with a FWE correction p<0.05. For subsequent analyses, we performed a nuisance regression on each of selected network time courses by partialing out the effect of our confounds of no interest (i.e. spike regressors and motion parameters). To benchmark our ICA-derived networks with those described in the existing literature, we compared repetition effects in the ICA derived DMN and MTL time series to those extracted from a meta-analytical mask for these networks. Both the meta-analytical and ICA timeseries were sensitive to the task manipulations showing a strong repetition effect. However, the ICA procedure extracted networks that were smaller in extent and more functionally specific. The ICA networks also showed stronger task-specific modulation effects (Data S1; Figure S6), consistent with data-driven derivation. Nonetheless, the broader convergence of effects demonstrates that the networks we focus on here are consistent with the canonical networks subject to extensive prior research.

Dynamic Causal Modeling (DCM)

To investigate the neuronal interactions between our selected cortical networks underlying task execution (i.e. effective connectivity) we used a deterministic bilinear DCM. DCM uses forward modeling at the level of the neuronal dynamics of a system through a bilinear differential equation. This model takes the form $\dot{z} = (A + \sum_{j=1}^{M} u_j B^j)z + Cu$ where $\dot{z}$ is the change in neural activity per unit time (i.e. derivative of neuronal state for each region), u introduces the experimental inputs, A is a matrix defining the intrinsic coupling between regions, B is a matrix representing modulatory effects of specific inputs on the connectivity between regions, and C is a matrix encoding the effect of the driving inputs u on those regions receiving those directly (see Methods S1).

Subject level model design and specification followed the procedure described in Zeidman et al.[91] A template model structure was built using the DCM graphical user interface in SPM. We then updated this template structure for each subject with specific task design matrices and ICA timeseries. To model the effects revealed by the GLM results we built our DCM to include input nodes that were category specific (i.e. scenes or objects) and the higher order networks that showed significant effects of repetition. The input nodes we selected for the DCM showed preferential activity for either scenes (PPA) or objects (LOC) stimuli. These input nodes are driven by the experimental conditions for scene or objects respectively (i.e. C matrix). The higher order networks that showed significant effects of repetition (MTL, DMN and SAL) were included to understand the modulating effect of repetition on the coupling between cortical networks (i.e. entries in B matrix). We built the directed graph of our DCM (i.e. A matrix) as a fully connected bidirectional graph except for connections between our two input nodes (i.e. LOC and MTL) which were left absent. We were specifically interested in the parameters modeling repetition-modulated effective connectivity between networks with colocalized AD pathologies (i.e. B matrix DMN to MTL, and MTL to DMN).

As noted above, DCM derives from a dynamic systems framework, and as such, each modeled directed connection represents the rate of change of neural activity in response to incoming signals (A and C matrix), or the up- or down modulation of that rate of change (B matrix). As such, it is standard to think of these effects as being excitatory (more positive rate of change = slower damping) or inhibitory (more negative rate of change = stronger damping). These modulatory parameters are rate constants that take the unit of Hertz and infer how afferent signal from one region leads to excitation or inhibition of another region.[92] For further theoretical explication and in silico validation see [93].

Parametric Empirical Bayes (PEB)

The PEB approach uses hierarchical Bayesian modeling within a random effects framework to estimate each parameter, assuming that each subject has the same model architecture but varying strengths of the connections within the group model (for recent review and validation see [94]). Bayesian Model Reduction (BMR) is first deployed to prune away parameters that don't contribute to model evidence (i.e. Free Energy). The BMR procedure iteratively tests different mixtures of connections and covariates and removes parameters that don't contribute to model evidence.[95] In this way only a single full DCM per subject is specified and the contribution of a given parameter within this full model is statistically assessed by comparing the evidence for models retaining this parameter vs. models without this parameter.[96] As model evidence (Free Energy) is a trade-off between the accuracy of the generative model (i.e. ability to predict observed BOLD data) and its complexity (the number of parameters and their divergence from their original values prior to model selection), this selection procedure yields a reduced model that provides the most parsimonious description of the observed data. Comparing the model evidence (Free energy) of all models in which a parameter is switched on vs. off yields a posterior probability (Pp) corresponding to each model's contribution to the overall model evidence. We present results of PEB parameters with very strong Bayesian evidence (Pp>0.99).

PEB estimation was run in SPM using the DCM Second Level interface as described in Zeidman et al.[94] To determine the effect of AD pathology on effective connectivity we included the following regressors within the PEB design matrix (i.e. X matrix); a.) a constant term, b.) mean centred continuous global Aβ and c.) mean centred continuous EC- tau. As our effective connectivity parameters of interest are related to how AD pathologies impact the processing of repetition, we focussed our investigation on the influence of these covariates (i.e. Aβ and EC-tau) on the modulation of coupling between the DMN and MTL (i.e. on the B matrix elements for DMN to MTL, and, MTL to DMN). Having entered a constant term and mean centred covariates of interest (i.e. EC-tau and Aβ) the parameters represent the mean coupling strength across the group between DMN and MTL when stimuli are repeated, and, the additive effect of each AD pathology on this common effect. In this way a negative value for the commonality represents an inhibitory connection (more damping) and a positive value for a covariate of interest represents an increase in excitation (less damping/ more excitation) scaled by the value of the covariate (i.e. Aβ or EC-tau).

In the framework of PEB, complex models that do not parsimoniously predict the data are down weighted, favouring a simpler model. Complex models have a greater chance to compete in the presence of precise, highly sampled data (where they have a higher chance or precisely predicted the data) but are less likely in noisy and/or downsampled data, where simpler models are favoured. In the setting of longer TR data, parameters that are retained in the model (or which show effects across groups of effects, such as the presence or absence of tau) must explain substantial variability in the data. In addition, we collapsed across stimulus category repetitions (i.e. combining object and scenes) resulting in 128 repetition trials across both runs for each participant. Taken together, the fitting procedure of DCM and the relatively large number of repetition trials in the data adds to the validity of model-based inference in this study.

Finally, we used cross validation to assess how the magnitude of the PEB effects related to the degree of variance in EC-tau pathology. Specifically, we ran a leave one out (LOO) validation using effects of interest (i.e. the modulation of the coupling between the DMN and MTL) to estimate out-of-sample outcomes of interest (i.e. EC-tau burden and accumulation). We ran the LOO in SPM using the DCM Second Level interface. We used LOO as it is a statistically robust approach to assess associations when sample sizes are small. We report the Pearson correlation coefficient (r) and the p value for the right tail correlation of model estimated vs. observed covariates of interest (i.e. EC-tau burden and rate of EC-tau accumulation).